Catalysis Today 413-415 (2023) 113958

Contents lists available at ScienceDirect

Catalysis Today

journal homepage: www.elsevier.com/locate/cattod

Kinetic model of photo-Fenton degradation of paracetamol in an annular reactor: main reaction intermediates and cytotoxicity studies

Bárbara N. Giménez [a], Leandro O. Conte [a], Francesca Audino [b], Agustina V. Schenone [a], Moisès Graells [b], Orlando M. Alfano [a], Montserrat Pérez-Moya [b,*]

[a] Instituto de Desarrollo Tecnológico para la Industria Química (INTEC), Consejo Nacional de Investigaciones Científicas y Técnicas (CONICET) and Universidad Nacional del Litoral (UNL), Ruta Nacional N◦ 168, 3000 Santa Fe, Argentina

[b] Chemical Engineering Department, Universitat Politècnica de Catalunya, Escola d'Enginyeria de Barcelona Est (EEBE), Av. Eduard Maristany, 16, Barcelona 08019, Spain

ARTICLE INFO

Keywords:
Acetaminophen
Photo-Fenton
Cytotoxicity
Hydroquinone
LVRPA
1,4-benzoquinone

ABSTRACT

A kinetic model derived from a simplified reaction sequence is proposed for the photo-Fenton degradation of Paracetamol (PCT), employing an annular photoreactor. The kinetic model explicitly included the effects of radiation absorption on pollutant degradation kinetics through the evaluation of the Local Volumetric Rate of Photon Absorption (LVRPA). Irradiated experiments achieved an average PCT conversion of 99.3% at 5 min of reaction, and a maximum of 69% of mineralization. Conversely, non-irradiated experiments reached an average PCT conversion of 86.6% at 5 min of reaction, and a maximum of 35% of mineralization. Kinetic parameters ($k_5 = 5.82 \times 10^9$, $k_6 = 3.01 \times 10^{10}$, $k_7 = 6.01 \times 10^{10}$ $M^{-1}s^{-1}$) were estimated employing a nonlinear, multi-parameter regression method, and the validated kinetic model was used to predict temporal variations of the concentrations of HP, PCT, and the main reaction intermediates: hydroquinone (HQ) and 1,4-benzoquinone (BQ). The root mean square error (RMSE) values obtained for HP, PCT, HP, HQ and BQ were 1.16×10^{-2}, 7.13×10^{-1}, 3.53×10^{-3}, 3.05×10^{-3} mM, respectively, showing a good agreement between experimental and predicted data. Moreover, the kinetic model was validated with a new set of experimental tests, confirming its predictive capacity. Beyond the degree of mineralization attained, additional cytotoxicity tests proved that the photo-Fenton process is effective in generating a non-toxic effluent under the operating variables investigated.

1. Introduction

For decades, new developments have been carried out to satisfy human beings' growing requirements, leading to the presence of different new chemical compounds in wastewater. The so-called "conventional" water treatments efficiently reduce the presence of N and P compounds, biological oxygen demand and pathogens, but they are not capable of degrading some of these new chemical substances [1]. Hence, these compounds (such as pharmaceuticals and personal care products (PPCPs), plasticizers, pesticides, surfactants, etc.) have been continuously introduced into natural environments for a long time, and that is why they are known collectively as Contaminants of Emerging Concern (CECs). Currently, CECs are not regulated in most of the world. Taking into account that many researchers consider that legislative intervention of governments would help to control this kind of contamination, efforts are being made in the European Union and North America to identify these CECs and reduce their release into the environment [2].

Due to the aforementioned, the need for more efficient methods for the treatment of environmental pollution has opened the field to investigate new technologies, such as Advanced Oxidation Processes (AOPs), aimed at achieving the decomposition of undesirable substances and avoiding at the same time the formation of toxic products [3]. AOPs have the potential to degrade, under environmental conditions, a wide range of hazardous compounds either partially (biodegradable products) or totally (CO_2 and H_2O). One of the most efficient AOPs is the photo-Fenton process [4]. Its mechanism is complex, but it can be described in a simplified way as the reaction between Fe^{2+} (catalyst) and H_2O_2 (oxidant), which generates Fe^{3+} and hydroxyl radicals ($HO^{\bullet}$). At pH < 3, Fe^{3+} remains dissolved and reacts with H_2O_2, generating Fe^{2+} and transforming the reaction system into an autocatalytic one. However, the reaction of Fe^{3+} with H_2O_2 occurs very slowly compared with the oxidation of Fe^{2+} by H_2O_2 [5]. Radiation accelerates Fenton

* Corresponding author.
E-mail address: montserrat.perez-moya@upc.edu (M. Pérez-Moya).

https://doi.org/10.1016/j.cattod.2022.11.019
Received 14 August 2022; Received in revised form 2 November 2022; Accepted 14 November 2022
Available online 15 November 2022

reactions, regenerating Fe^{2+} and producing more $HO^{\bullet}$ [6]. Since the photo-Fenton process can be carried out at wavelengths up to approximately 580 nm, it can be induced by solar radiation as a renewable energy source, making the process both economically and environmentally sustainable [7].

To study the intrinsic phenomena implied in the AOPs treatment technologies, particularly in the case of Fenton and photo-Fenton processes, the bibliography reports different approaches. There are a lot of empirical models (regression models), which are generally good for a given range of experimental working conditions but are not valid as predictive tools for different reactor configurations [8–10]. However, there are a small number of kinetic models that from a reaction scheme propose the resolution of the mass balance and radiative energy equations through the evaluation of the local volumetric rate of photon absorption (LVRPA) [11–13]. It is important to note that the development of these types of models is of great significance since allow not only to make predictions associated with the behaviour of reaction systems but also to extrapolate the results to larger scales of operation (pilot plant and industrial reactors).

In this work, the analgesic Paracetamol (PCT) is used as a model contaminant. It is a biologically active substance, toxic to various organisms (mainly aquatic) and even human beings, mainly due to the presence of phenolic groups [14]. Moreover, the PCT is one of the most widely used drugs to relieve fever and pain [15], and is recommended to treat mild symptoms of coronavirus disease (COVID-19) [16] causing large amounts of this compound to be discharged into water systems (low absorption in the human body) [17]. From this, different amounts of this compound were detected in effluents of hospitals, pharmaceutical industries (up to 294 mg L^{-1} [18,19]), and urban sewage treatment plants.

This work aims to improve the previous kinetic model [20] derived from a simplified reaction sequence, to study the Fenton and photo-Fenton degradation of Paracetamol (PCT) using an annular photoreactor. In this sense, the behaviour of the main reaction intermediates, hydroquinone (HQ) and 1,4-benzoquinone (BQ), was also studied. Furthermore, to assess the toxicity resulting from the generation of these reaction intermediates, cytotoxicity assays were performed with VERO cells throughout the reaction time. The proposed kinetic model explicitly considers the effects of radiation absorption on the contaminant degradation kinetics by evaluating the LVRPA. The unknown kinetic parameters (only three) were estimated by fitting the model to experimental data. Furthermore, the model was validated using a new set of experimental data.

Finally, a cytotoxicity study completes the analysis of the efficiency of the photo-Fenton degradation of the PCT. For this purpose, VERO cells (which come from an African green monkey kidney) were employed as a model system, since these cells could represent a more adequate system when evaluating the toxicity of superior organisms. Hence, the viability of VERO cells was studied not only in the final generated effluent of reaction but also during the entire process of the PCT abatement.

2. Materials and methods

2.1. Chemicals and reagents

Analytical grade reagents were used as well as deionised water as water matrix and milli Q grade water as HPLC mobile phases. PCT (98% purity) was purchased from Sigma-Aldrich. Hydroquinone and 1,4-benzoquinone (HQ and BQ, both 99% purity) were obtained from Fluka. Hydrogen peroxide (HP, 33% w/w) was purchased from Panreac Química SLU. The salt $Fe_2SO_4.7\ H_2O$ (Merck, pro-analysis) was used as a Fe^{2+} source. Ascorbic acid (purity > 99%) and 0.2% 1,10-phenanthroline, both used to perform iron species measurements, were purchased from Riedel de Haën and Scharlab, respectively. Finally, Hydrogen chloride (HCl, 37%) or pH adjustment and methanol (HPLC grade) were obtained from J.T. Baker.

2.2. Analytical determinations

PCT and its reaction intermediates (BQ and HQ) were determined using an HPLC Agilent 1200 series with UV-DAD array detector (set at 243 nm), with an Akady 5 μm C-18 150 × 4.6 mm column. The eluent was a mixture of methanol:water (25:75) flowing at 0.4 mL min^{-1}, and 20 μL samples were injected by a manual injector. All the samples were treated with 0.1 M methanol, in proportion 50:50, to stop the reaction. HP, Fe^{2+} and Total Fe were determined using a UV/Vis spectrophotometer (Hitachi U-2001). In the case of iron, samples for Fe^{2+} and Total Fe were analysed by means of the colorimetric method with 1,10-phenanthroline at 510 nm. Samples for Total Fe determination were pretreated with ascorbic acid to convert all the ferric ions to ferrous ions. HP was monitored through the measurement of the absorption at 450 nm of the complex formed after its reaction with ammonium metavanadate [21]. Samples for determination of TOC were taken and refrigerated (to slow down any further degradation of the organic matter) until their analysis through a VCHS/CSN TOC analyser (Shimadzu).

2.3. Experimental device and procedure

The experiments were carried out in a glass annular photoreactor (1.5 L) with external recycling, connected to a glass jacketed reservoir tank (9 L). The experimental system was completed with a pH-meter, a flowmeter, and a thermostatic bath for temperature control. A pumping system allows keeping a constant recirculation flow of 12 L min^{-1}, which ensures perfect mixing. The photoreactor was equipped with an Actinic BLTL-DK 36 W/10 1SL lamp (UVA-UVB, $\varnothing$ = 28 mm and L = 589.8 mm). The lamp spectral irradiance can be found in the "Supplementary Material" (Fig. S2). The total reaction volume (V_{tot}) was 15 L and the irradiated one (V_{irr}) was 1.5 L (that is, 10% of the total volume). A detailed description of the experimental system can be found in Yamal-Turbay et al. [22]and in the Fig. S1 provided in the "Supplementary Material. The incident photon power, E = 3.36 × 10^{-4} Einstein min^{-1} (between 300 and 420 nm) was measured using potassium ferrioxalate actinometry [22].

Each experiment began with the filling of the glass reservoir with 10 L of deionised water and then adding 4.9 L of the aqueous solution containing PCT. The pH was adjusted to 2.8 ± 0.1 with 37% hydrogen chloride (J.T. Baker Inc.) and 0.1 L of the aqueous solution containing iron sulphate was added. Then, an aliquot was taken to determine the initial concentrations of the iron species. Finally, to start the experiment, the HP solution was added. In the case of the experiments carried out with radiation, and to allow the stabilization of the emitted radiation, the lamp was turned on 10 min before adding the HP. Total reaction time was set at 75 min for all the experiments carried out.

The treated sample consisted of deionised water spiked with the contaminant. Initial PCT concentration was set at 40 mg L^{-1} in all the experiments. The effect of the following operative variables was tested on PCT degradation: Fe^{2+} initial concentration ($[Fe^{2+}]^0$, between 5 and 10 mg L^{-1}), HP initial concentration ($[HP]^0$, between 94.5 and 378 mg L^{-1}), and UV-radiation (ON or OFF). It was decided to set these particular operating parameters considering previous studies [20]. The set of experimental tests carried out, with their corresponding operating conditions of initial concentrations of catalyst and oxidant, and with or without radiation, is presented in Table 2 (see Section 4.1 Experimental Results).

Finally, a set of blank assays was performed in order to identify the effect of each reagent on the degradation and mineralization of PCT. The three blank assays undertaken correspond to only irradiation, only Fe^{2+} at a concentration of 10 mg L^{-1} and only H_2O_2 at a concentration of 756 mg L^{-1}. Results demonstrate that the reagents alone produce no

Table 1
Simplified reaction scheme of PCT photo-Fenton degradation.

N°	Reaction Step	Kinetic Constant (M^{-1} s^{-1})
1	$Fe^{2+} + H_2O_2 \xrightarrow{k1} Fe^{3+} + OH^- + HO^\bullet$	$k_1 = 147.29$[a]
2	$Fe^{3+} + H_2O_2 \xrightarrow{k2} Fe^{2+} + H^+ + HO_2^\bullet$	$k_2 = 3.16$[a]
3	$Fe^{3+} + H_2O \xrightarrow{\Phi_{Fe^{2+}}} Fe^{2+} + H^+ + HO^\bullet$	$\Phi_{Fe^{2+}} = 0.21$mol Einstein^{-1} [a]
4	$H_2O_2 + HO^\bullet \xrightarrow{k_4} HO_2^\bullet + H_2O$	$k_4 = 7.00 \times 10^7$[a]
5	$PCT + HO^\bullet \xrightarrow{k_5} HQ$	k_5[b]
6	$HQ + HO^\bullet \xrightarrow{k_6} BQ$	k_6[b]
7	$BQ + HO^\bullet \xrightarrow{k_7} P_i$	k_7[b]

[a] values taken from Audino et al. [20].
[b] values estimated in this research work.

Table 2
Experimental conditions for each experimental run (Runs 1–8 and Runs 1_V* and 2_V*), PCT conversion at 5 (X_{PCT}^{5min}), and 10 (X_{PCT}^{10min}) min of reaction, and TOC conversion after 75 min of reaction (X_{TOC}^{75min}).

Run	$[Fe^{2+}]^0$ (mgL^{-1})	$[HP]^0$ (mgL^{-1})	Radiation	X_{PCT}^{5min} (%)	X_{PCT}^{10min} (%)	X_{TOC}^{75min} (%)
#1	5	94.5	OFF	80.4	96.0	29.3
#2	5	189	OFF	84.7	96.6	30.6
#3	7.5	378	OFF	84.5	97.1	35.7
#4	10	189	OFF	96.9	100	33.3
#5	5	189	ON	97.3	100	55.2
#6	5	378	ON	100	100	69.6
#7	7.5	94.5	ON	100	100	33.6
#8	10	378	ON	100	100	68.7
#1_V[a]	7.5	189	ON	97.3	100	55.2
#2_V[a]	7.5	189	OFF	96.9	100	32.3

[a] Runs for model validation at central point conditions of $[Fe^{2+}]^0$ and $[HP]^0$.

PCT degradation, except in the case of H_2O_2 alone, which led to only 18% degradation after 90 min treatment. Moreover, PCT and TOC remained almost constant under UV radiation (300–420 nm) tests.

2.4. Toxicity test

The acute toxicity was monitored during the oxidation process. Cytotoxicity tests based on cell lines culture were carried out, employing VERO cells (ATCC®, Manassas, VA, USA). For this purpose, the methodology described by Audino et al. [23] was employed. In brief, aqueous samples were taken at predefined times during the treatment by Fenton and photo-Fenton processes, at different operational conditions and were evaluated at serial one-third dilutions. A control of maximum cell growth (achieved culturing the cells in medium alone), and a control to evaluate the effect of the aqueous dilution of the medium, were performed. Every sample was evaluated in triplicate, on independent plates. Cytotoxicity was assessed by measuring the viability of the cells (determined by the MTT method) [24] exposed to the contaminant and its by-products.

3. Modelling

A kinetic model that describes the degradation of PCT and its intermediates, through the homogeneous Fenton and photo-Fenton processes, was developed. Table 1 represents the reaction mechanism proposed, based on a simplified scheme extracted from the analysis of more complex and specific reaction schemes [25,26]. The above-mentioned scheme also includes the formation and degradation of two PCT reaction intermediates, 1,4-benzoquinone (BQ), and hydroquinone (HQ), which were identified and quantified in the present work [27].

The simplified reaction scheme was made based on a series of hypotheses [28]: i) for highly reactive radicals (i.e. HO•), the steady-state approximation (SSA) was applied; ii) the only oxidizing species considered were HO•, since radical HO_2• is far less reactive than HO• [29,30]; iii) radical–radical termination reactions are neglected compared to the propagation/consumption ones; iv) reactions of Fe^{2+} with HO• are neglected due to the low iron concentrations employed in this experimental system; v) the oxygen concentration is always in excess.

Then, these assumptions allowed to obtain the reaction rate expressions, for the following studied species (PCT, HP, Fe^{2+}, Fe^{3+}, HQ and BQ) (Eqs. 1–7):

$$R_{PCT}(\underline{x},t) = -k_5[\mathrm{PCT}][HO^\bullet] \tag{1}$$

$$R_{HP}\left(\underline{x},t\right) = -k_1\left[Fe^{2+}\right][HP] - k_2\left[Fe^{3+}\right][HP] - k_4[HP][HO^\bullet] \tag{2}$$

$$R_{Fe^{2+}}\left(\underline{x},t\right) = -k_1\left[Fe^{2+}\right][HP] + k_2[Fe^{3+}][HP] + \Phi_{Fe^{2+}}\sum_\lambda e_\lambda^a\left(\underline{x},t\right) \tag{3}$$

$$R_{Fe^{3+}}\left(\underline{x},t\right) = -R_{Fe^{2+}}(\underline{x},t) \tag{4}$$

$$R_{HQ}\left(\underline{x},t\right) = k_5[\mathrm{PCT}][HO^\bullet] - k_6[HQ][HO^\bullet] \tag{5}$$

$$R_{BQ}\left(\underline{x},t\right) = k_6[HQ][HO^\bullet] - k_7[\mathrm{BQ}][HO^\bullet] \tag{6}$$

$$R_{HO^\bullet}\left(\underline{x},t\right) = k_1\left[Fe^{2+}\right][HP] + \Phi_{Fe^{2+}}\sum_\lambda e_\lambda^a\left(\underline{x},t\right) - k_4[HP][HO^\bullet] - k_5[\mathrm{PCT}][HO^\bullet] - k_6[HQ][HO^\bullet] - k_7[BQ][HO^\bullet] \tag{7}$$

Here, $\Phi_{Fe^{2+}}$ is the wavelength-averaged primary quantum yield and $\sum_\lambda e_\lambda^a\left(\underline{x},t\right)$ the LVRPA in the photoreactor extended to polychromatic radiation by performing the integration over all useful wavelengths (λ: 300–420 nm).

Note that Eqs. (1–7) can be generalized by using the following matrix representation:

$$\boldsymbol{R}_i\left(\underline{x},t\right) = \boldsymbol{R}_i^{\boldsymbol{T}}(t) + \boldsymbol{R}_i^{\boldsymbol{irr}}(\underline{x},t) \tag{8}$$

The first term on the right-hand side of Eq. (8) corresponds to the thermal reaction rate (function only of time, t), and the second one represents the irradiated reaction rate (function of the position in the photoreactor, $\underline{x}$ and the time, t).

The mass balance for the well-stirred isothermal annular photoreactor in which the kinetic studies were carried out is represented by the following set of first order, ordinary differential equations (Eq. 9) with their corresponding initial conditions (Eq. 10) for all the chemical species "i" considered (PCT, HP, Fe^{2+}, Fe^{3+}, HQ and BQ):

$$\frac{d\boldsymbol{C}_i(t)}{dt} = \frac{V_{tot} - V_{irr}}{V_{tot}}\boldsymbol{R}_i^{\boldsymbol{T}}(t) + \frac{V_{irr}}{V_{tot}}\left\langle \boldsymbol{R}_i^{\boldsymbol{irr}}(\underline{x},t)\right\rangle_V \tag{9}$$

$$\boldsymbol{C}_i = \boldsymbol{C}_i^{\boldsymbol{0}} \quad t_0 = 0 \tag{10}$$

Applying the steady-state approximation (SSA) to the radical $HO^\bullet$ ($R_{HO^\bullet}\left(\underline{x},t\right) = 0$ in Eq. 7), the expression corresponding to $[HO^\bullet]$ is obtained. Replacing this expression into each of the Eqs. 1 to 6, and then replacing the expressions obtained in Eq. (9), the system of ordinary differential equations that models the studied system is achieved (eqs. A.1 to A.5, Appendix A).

Finally, following the assumptions adopted by Audino et al. [20], it is

possible to calculate the average volumetric rate of photon absorption inside the photoreactor for polychromatic radiation ($\left\langle \sum_{\lambda} e^{a}_{\lambda}\left(\underset{\sim}{x},t\right)\right\rangle_{V_{irr}}$), through the numerical integration of Eq. (11).

$$\left\langle \sum_{\lambda} e^{a}_{\lambda}\left(\underset{\sim}{x},t\right)\right\rangle_{V_{irr}} = \frac{2\pi}{V_{irr}}\int_{0}^{L}\int_{r_{int}}^{r_{ext}} e^{a}_{\lambda}\left(\underset{\sim}{x},t\right)\; r\; dr\; dz = \frac{2\pi}{V_{irr}}\int_{0}^{L}\int_{r_{int}}^{r_{ext}}\left[\kappa_{\lambda}\left(\underset{\sim}{x},t\right)\frac{P_{\lambda,s}}{2\pi L_{L}}\int_{\Theta_1}^{\Theta_2} exp\left[-\frac{\kappa_{T,\lambda}\left(\underset{\sim}{x},t\right)(r_i - r_{int})}{\cos\theta}\right]d\theta\right] r\; dr\; dz \tag{11}$$

Here, $P_{\lambda,s}$ is the lamp spectral power emission (provided by the lamp supplier), $\kappa_{\lambda}\left(\underset{\sim}{x},t\right)$ the volumetric absorption coefficient of the reacting species, $\kappa_{T,\lambda}\left(\underset{\sim}{x},t\right)$ the volumetric absorption coefficient of the medium, r the radius, and L_L the useful length of the lamp. Also, r_{int} and r_{ext} are the internal and external radio of the annular photoreactor, respectively.

3.1. Kinetic parameter estimation

An optimization procedure was employed to provide the values of kinetic constants (k_5, k_6 and k_7) that minimize the differences between the predicted concentrations and the corresponding experimental values, for each stable species i considered (PCT, HP, HQ and BQ). The theoretical values were obtained by solving the system of ordinary differential equations (Eqs. 9 and 10), utilizing GNU Octave (Version 5.2.0) software. Making use of the complete set of experimental data to fit the proposed kinetic model, the three rate constants (k_5, k_6, and k_7) were estimated, employing a nonlinear least-square objective function (Newton Gauss-Marquardt algorithm). Details about the numerical structure to obtain the kinetic parameters and the simulations of the experimental data can be found in the Fig. S3 in the Supplementary Material. Finally, the root mean square error (RMSE), calculated for each chemical species i with Eq. (12), was used to evaluate the model accuracy.

$$RMSE_i = \sqrt{\frac{\left(C_{i,exp} - C_{i,mod}\right)^2}{n}} \tag{12}$$

Here, $C_{i,exp}$ and $C_{i,mod}$ are the experimental data and those predicted by the model, respectively, and n is the total number of samples (whole set of experimental runs).

4. Results

4.1. Experimental results

Table 2 details the operating conditions (iron and hydrogen peroxide concentrations and radiation ON or OFF) for each of the experimental tests carried out (Runs 1–8 and Runs 1_V* and 2_V*). In addition, the experimental PCT conversions obtained for 5 (X^{5min}_{PCT}) and 10 (X^{10min}_{PCT}) minutes of reaction are presented, as well as the conversion levels obtained for total organic carbon (TOC) after 75 min of reaction (X^{75min}_{TOC}).

Examining the experimental PCT conversion at 5 min of reaction (X^{5min}_{PCT}), all the runs carried out in the presence of radiation reached close to 100% conversion of PCT. In contrast, runs under Fenton condition have a maximum conversion of 96.9% (run #4, 10_189_OFF) and a minimum conversion of 80.4% (run #1, 5_94.5_OFF). These results demonstrate the importance of radiation in the studied system. Additionally, if runs #2 (5_189_OFF, $X^{5min}_{PCT} = 84.7\%$) and #5 (5_189_ON, $X^{5min}_{PCT} = 97.3\%$) are analysed, which have identical initial conditions of Fe^{2+} and HP concentrations, but were carried out in the absence and presence of radiation (respectively), it is observed that with the photo-Fenton system a conversion difference of almost 15% higher than with the dark reaction is achieved. Moreover, run #2 (Fenton) takes twice as many minutes in reaction time (10 min) to reach a PCT conversion ($X^{10min}_{PCT} = 96,6\%$) close to the X^{5min}_{PCT} of run #5 ($X^{5min}_{PCT} = 97,3\%$).

TOC conversions (X_{TOC} (%)) were also estimated after 75 min of reaction (see Table 2). In the case of reactions carried out under dark conditions (run #1 to #4), the maximum TOC conversion achieved was only 35.7% (run #3), being minimal (29.3%) for conditions of run #1 (5_94.5_OFF), where the lowest dosage of oxidizing agent and catalyst have been used.

However, in presence of radiation, it can be observed that the degree of TOC conversion achieved was higher than 33.5% for all the conditions studied after 75 min of reaction, being maximum (69.6%) for the experimental run #6 (5_378_ON). Therefore, the performance of the process in terms of mineralization levels achieved is substantially improved by radiation.

4.2. Model results

Firstly, it is important to note that the values of the estimated kinetic parameters: $k_5 = 5.82 \times 10^9$, $k_6 = 3.01 \times 10^{10}$, $k_7 = 6.01 \times 10^{10}$ $M^{-1}s^{-1}$, are close to those found in the specific literature [25,31,32]. Moreover, the relatively low RMSE values obtained (in the same order of magnitude as the experimental error) using Eq. (12): 1.49×10^{-2}, 9.00×10^{-1}, 6.33×10^{-3}, 5.62×10^{-3} mM for PCT, HP, HQ and BQ, respectively, show that the kinetic model adequately describes the behaviour of the reacting system. Furthermore, normalizing the RMSE values of the species initially present in the system (PCT and HP) according to its initial experimental concentration, low errors of 5.63% and 8.10% are reached, which again represents the efficiency of the model.

From Fig. 1a and b, increasing the oxidant agent concentration $[HP]^0$ from 94.5 to 189 mg L^{-1} did not cause a higher degradation rate or final conversion of both the PCT and its intermediates. For these dark Fenton reactions (run #1 and #2), an excess of HP can enhance the consumption of hydroxyl radical, according to (Eq. 13) [33].

$$H_2O_2 + OH\bullet \rightarrow HO_2^-\bullet + H_2O \tag{13}$$

Under operating conditions of Fig. 1c and d, with an initial HP concentration of 378 mg L^{-1}, but with different $[Fe^{2+}]^0$ (run #6: 5 mg L^{-1} and run #8: 10 mg L^{-1}), it can be observed the beneficial effect of increasing the initial concentration of iron on the by-product's degradation. Here, the time required to achieve the total removal of the intermediates is reduced by 50% when increasing $[Fe^{2+}]^0$ from 5 to 10 ppm.

Finally, a new set of experimental runs at central point conditions of $[Fe^{2+}]^0$ and $[HP]^0$ were performed to validate the kinetic model (runs #1_V and #2_V, Table 2). Fig. 2a and b show a good agreement between the experimental data and the predicted concentrations for validation assay conditions (RMSE values obtained: 1.16×10^{-2}, 7.13×10^{-1}, 3.53×10^{-3}, 3.05×10^{-3} mM for PCT, HP, HQ and BQ, respectively).

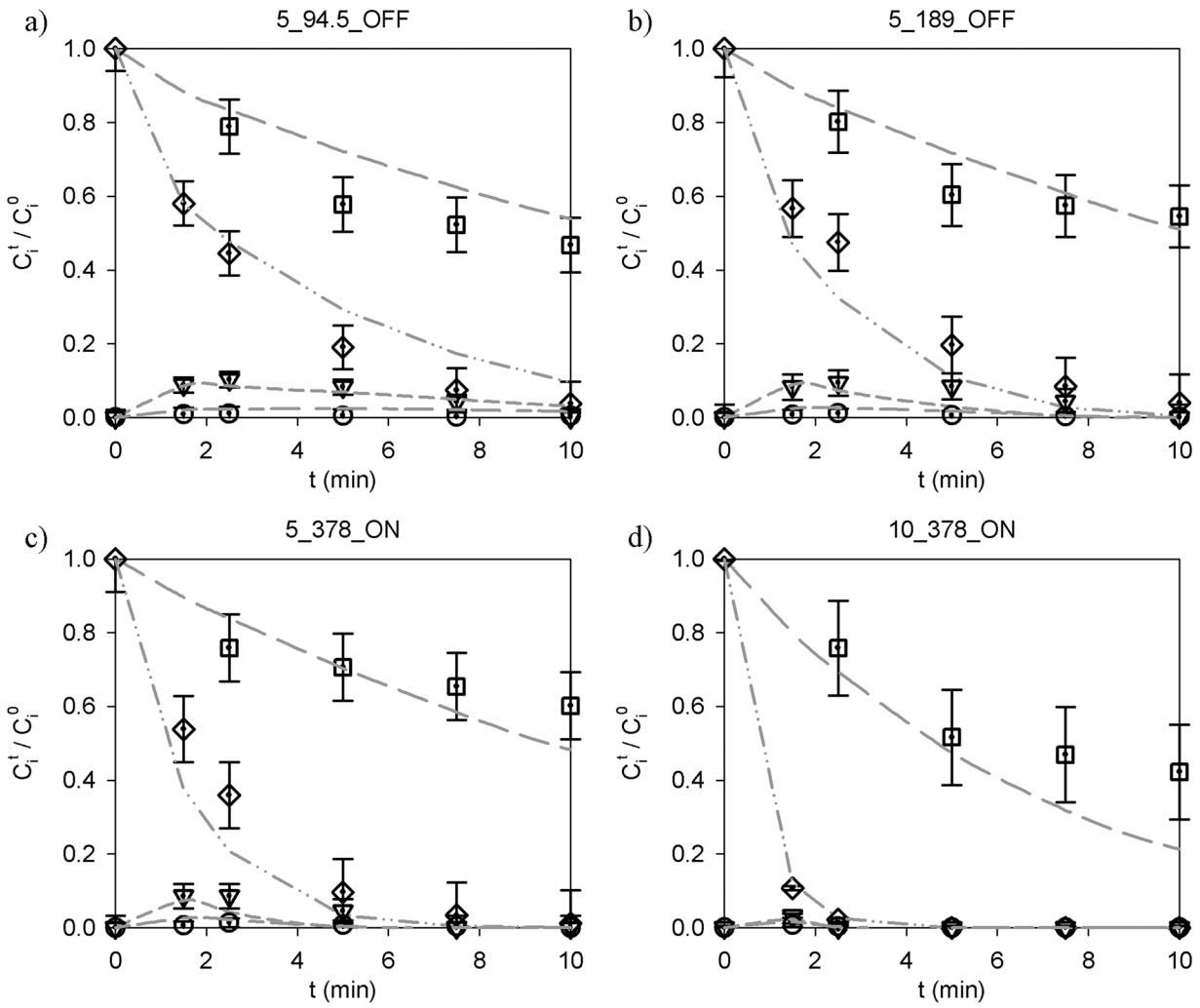

Fig. 1. Experimental and model results for PCT, HP, HQ, and BQ species, in relative concentrations. a) $[Fe^{2+}]^0 = 5$ mg L^{-1}, $[HP]^0 = 94.5$ mg L^{-1}, radiation: OFF; b) $[Fe^{2+}]^0 = 5$ mg L^{-1}, $[HP]^0 = 189$ mg L^{-1}, radiation: OFF; c) $[Fe^{2+}]^0 = 5$ mg L^{-1}, $[HP]^0 = 378$ mg L^{-1}, radiation: ON; d) $[Fe^{2+}]^0 = 10$ mg L^{-1}, $[HP]^0 = 378$ mg L^{-1}, radiation: ON. Keys: PCT = diamond, HP = square, HQ = triangle down, BQ = circle, experimental results; and PCT = dash-dot line, HP = long dash line, HQ = short dash line, BQ = short-long line, model results.

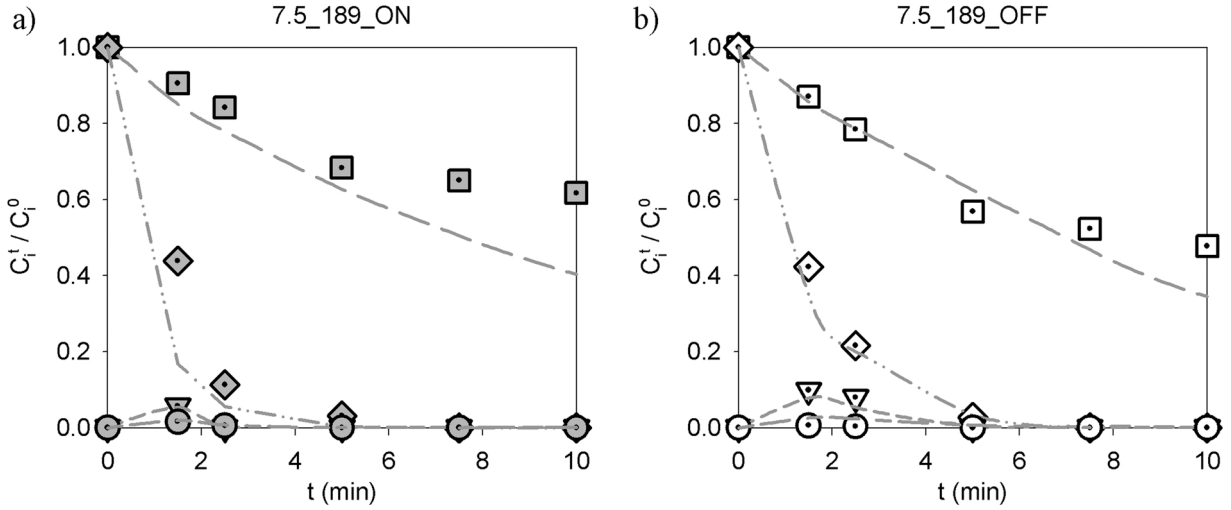

Fig. 2. Experimental and model results for PCT, HP, HQ, and BQ species, in relative concentrations for the validation assays: a) $[Fe^{2+}]^0 = 7.5$ mg L^{-1}, $[HP]^0 = 189$ mg L^{-1}, radiation: ON; b) $[Fe^{2+}]^0 = 7.5$ mg L^{-1}, $[HP]^0 = 189$ mg L^{-1}, radiation: OFF. Keys: PCT = diamond, HP = square, HQ = triangle down, BQ = circle, experimental results; and PCT = dash-dot line, HP = long dash line, HQ = short dash line, BQ = short-long line, model results.

Therefore, the proposed kinetic model is adequate to predict the temporal variations of the PCT, HP and main reaction intermediates concentrations, using the Fenton and photo-Fenton process in the annular photoreactor.

4.3. Toxicity results

Different cell types may be selected for studying toxicity. The most common options are *E. Coli* and *S. Aureus* bacteria. However, both species have been shown to be capable of metabolizing PCT and using it as a carbon source for its growth. Therefore, VERO cells were selected for performing the toxicity assays since they have shown to offer greater sensitivity to PCT and its by-products [23].

The LC_{50} value for PCT was determined and resulted to be considerably high (>1000 mg L^{-1}), showing that the selected initial concentration of PCT (40 mg L^{-1}) does not have a toxic effect on VERO cells. Fig. 3 shows the cytotoxicity results, as the temporal evolution of VERO cells viability for the entire reaction time (75 min) along with the temporal evolution of de HP concentration.

Certainly, cells viability may result from a combined toxic effect of different chemical species in the reaction media. This deserves further discussion. On one hand, the intermediates HQ and BQ could be suggested as affecting viability. This can be discarded as it is proved (Figs. 1 and 2) that these species have a very short presence in the media, and they remain undetectable after 6 min. On the other hand, HP requires a deeper analysis of the data. Towards this end, Fig. 3 displays the evolution of HP concentration parallel to cell viability. All cases (a,b,c,d) show there is no HP by the end of the reaction time. They also show that HP is consumed earlier in cases c and d, because of light as it should be expected. These two cases reveal very high cell viability despite the presence or absence of HP, which allows concluding the irrelevant effect of HP to toxicity.

In Fig. 3a, a marked decrease in the viability of the cells is observed from the beginning to the end of the reaction, only recovering some viability at t = 25 min, although not 100%. Therefore, it is concluded that it is not safe to apply the proposed treatment at low concentrations of Fenton reagents without radiation.

Similarly, in Fig. 3b it can be observed that cell viability begins to decrease after 25 min of reaction, being recovered only towards the end of the process. This implies that, under these concentrations of Fenton reagents and without radiation, it would only be safe to stop the reaction after t = 60 min. Between 15 and 20 min reaction time, cell viability is also important, but if the results of TOC conversion are analysed together with this toxicity assay, in the same time lapse, the X_{TOC} achieved is 14% on average (results not shown), but at the end of the reaction (75 min) it is higher than 35% (Table 2).

For Fig. 3c the presence of radiation greatly improves the cytotoxicity profile presented by the system, where cell viability never drops to less than 20%, Furthermore, towards the end of the reaction, almost 100% viability is recovered. In addition, after 30 min of reaction, the X_{TOC} reached a plateau at the end of the reaction at a value of around 34% (Table 2).

Finally, in Fig. 3d a good cytotoxicity profile is observed throughout the reaction time and, most importantly, at the end of the degradation process, 100% recovery of cell viability is obtained. However, if we consider the X_{TOC}, it reaches a maximum value of almost 70% (Table 2)

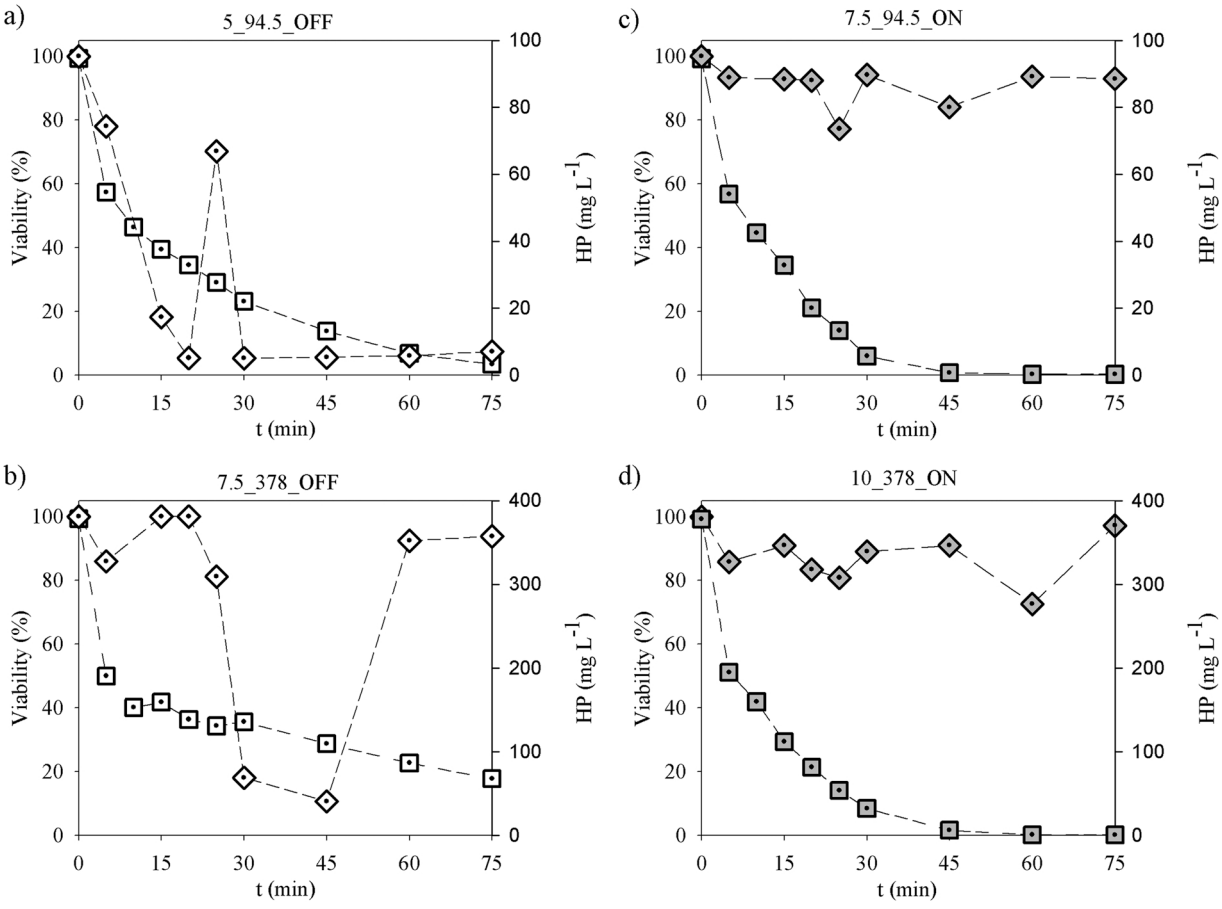

Fig. 3. Cytotoxicity temporal evolution (diamond) and HP concentration (square). a) run #1: most adverse operational conditions for the reaction; b) run #3: Fenton reaction, medium $[Fe^{2+}]^0$ and high $[HP]^0$ operational conditions; c) run #7: photo-Fenton reaction, medium $[Fe^{2+}]^0$ and low $[HP]^0$ operational conditions; d) run #8: more favourable operational conditions for the reaction.

towards the end of the process (t = 75 min).

Now, analysing together the results previously stated about TOC conversion and cytotoxicity for runs #7 and #8, it can be deduced that just some of the by-products have toxic effects on VERO cells, since both experiments reached a very different X_{TOC} but very similar viability levels towards the end of the reaction. This could be explained considering the nature of the formed by-products since the oxidation of the CECs could produce some intermediaries that are more hydrophilic than their parent compounds. This would reduce the ability of these compounds to penetrate through cell membranes, therefore resulting in less toxic for VERO cells [34].

5. Conclusions

A kinetic model was presented and experimentally validated to describe the Fenton and photo-Fenton degradation of Paracetamol and its main degradation by-products, hydroquinone, and 1,4-benzoquinone, in an annular photoreactor. The proposed kinetic model, derived from a simplified reaction sequence, explicitly included the effects of radiation absorption on the pollutant degradation kinetics through the evaluation of the Local Volumetric Rate of Photon Absorption. Using a nonlinear multi-parameter optimization procedure with only a minimum of three estimated kinetic constants, it was demonstrated that the model presented a good agreement between the experimental data and the predicted concentrations, not only of Paracetamol and hydrogen peroxide but also of hydroquinone and 1,4-benzoquinone. From a new set of experimental data, the kinetic model was validated confirming that the estimated parameters are adequate to represent the behaviour of the photo-Fenton process under the operating conditions tested.

Furthermore, to assess the environmental implications of the photo-Fenton process, a cytotoxicity study was conducted with VERO cells throughout the entire reaction time. Analysing these results, it was possible to observe that the presence of radiation in the system led to the production of a less toxic effluent compared to the non-irradiated systems, since a viability of over 95% was obtained for the photodegradation tests. Additionally, the increase in iron and hydrogen peroxide concentration produced an improvement in the cytotoxicity profiles of the system in contrast with the toxicity levels achieved in the Fenton run with the most adverse operational conditions. From the cytotoxicity results together with the experimental results of the total organic carbon conversion, it was possible to observe that some of the by-products generated from the reaction can have toxic effects on the VERO cells. These results demonstrate the importance of evaluating the toxicity throughout the reaction time, to define when it may be convenient to stop the contaminant degradation reaction.

CRediT authorship contribution statement

Conceptualization: Ideas; formulation or evolution of overarching research goals and aims. *Alfano Orlando M., P é rez-Moya Montserrat, Conte Leandro O, Graells Moisès.* Methodology Development or design of methodology; creation of models. *P é rez-Moya Montserrat, Conte Leandro O, Graells Moisès, Alfano Orlando M.* Software Programming, software development; designing computer programs; implementation of the computer code and supporting algorithms; testing of existing code components. *Conte Leandro O.* Validation Verification, whether as a part of the activity or separate, of the overall replication/ reproducibility of results/experiments and other research outputs. *Audino Francesca, Graells Moisès, P é rez-Moya Montserrat.* Formal analysis Application of statistical, mathematical, computational, or other formal techniques to analyze or synthesize study data. Investigation Conducting a research and investigation process, specifically performing the experiments, or data/evidence collection. *Audino Francesca, P é rez-Moya Montserrat, Giménez Bárbara N., Schenone Agustina V.* Resources Provision of study materials, reagents, materials, patients, laboratory samples, animals, instrumentation, computing resources, or other analysis tools. *Conte Leandro O., P é rez-Moya Montserrat.* Data Curation Management activities to annotate (produce metadata), scrub data and maintain research data (including software code, where it is necessary for interpreting the data itself) for initial use and later reuse. *Giménez Bárbara N., Schenone Agustina V., Conte Leandro O.* Writing - Original Draft Preparation, creation and/or presentation of the published work, specifically writing the initial draft (including substantive translation). *Giménez Bárbara N., Conte Leandro O., Schenone Agustina V., Alfano Orlando M.* Writing - Review & Editing Preparation, creation and/or presentation of the published work by those from the original research group, specifically critical review, commentary or revision – including pre-or post-publication stages. *Conte Leandro O., Graells Moisès, Alfano Orlando M., P é rez-Moya Montserrat.* Visualization Preparation, creation and/or presentation of the published work, specifically visualization/ data presentation. *Conte Leandro O., Schenone Agustina V., Giménez Bárbara N.* Supervision Oversight and leadership responsibility for the research activity planning and execution, including mentorship external to the core team. *P é rez-Moya Montserrat, Conte Leandro O.* Project administration Management and coordination responsibility for the research activity planning and execution. *Conte Leandro O., P é rez-Moya Montserrat* Funding acquisition Acquisition of the financial support for the project leading to this publication. *Graells Moisès, Alfano Orlando M.*

Declaration of Competing Interest

The authors declare that they have no known competing financial interests or personal relationships that could have appeared to influence the work reported in this paper.

Data availability

Data will be made available on request.

Acknowledgements

This work was supported from the Spanish "Ministerio de Ciencia e Innovación" and the European Regional Development Fund, both funding the research Project CEPI (PID2020–116051RB-I00) which is fully acknowledged. The authors are also grateful to Universidad Nacional del Litoral (UNL), Consejo Nacional de Investigaciones Científicas y Técnicas (CONICET) 50620190100040LI and Agencia Nacional de Promoción Científica y Tecnológica (ANPCyT, PICT Nº2018-01415 and Nº2018-02346) of Argentina for the financial support.

APPENDIX A

First-order ordinary differential equations that model the well-stirred isothermal annular photoreactor used in this research work.

$$\frac{dC_{PCT}}{dt} = \left\{ \frac{V_{irr}}{V_{tot}} \left[-k_5[\mathrm{PCT}] \frac{k_1\left[Fe^{2+}\right][HP] + \Phi_{Fe^{2+}} \left\langle \sum_{\lambda} e^{a}_{\lambda}\left(\bar{x}, t\right) \right\rangle_{V_{irr}}}{k_4[HP] + k_5[\mathrm{PCT}] + k_6[HQ] + k_7[BQ]} \right] \right\} + \left\{ \frac{V_{tot} - V_{irr}}{V_{tot}} \left[-k_5[\mathrm{PCT}] \frac{k_1[Fe^{2+}][HP]}{k_4[HP] + k_5[\mathrm{PCT}] + k_6[HQ] + k_7[BQ]} \right] \right\} \quad (A.1)$$

$$\frac{dC_{HP}}{dt} = \left\{ \frac{V_{irr}}{V_{tot}} \left[-k_1\left[Fe^{2+}\right][HP] - k_2\left[Fe^{3+}\right][HP] - k_4[HP]\frac{k_1[Fe^{2+}] \quad [HP] + \Phi_{Fe^{2+}}\left\langle \sum_\lambda e_\lambda^a\left(\underset{-}{x},t\right)\right\rangle_{V_{irr}}}{k_4[HP] + k_5[\mathrm{PCT}] + k_6[HQ] + k_7[BQ]} \right] \right\} + \left\{ \frac{V_{tot} - V_{irr}}{V_{tot}} \left[-k_1\left[Fe^{2+}\right][HP] - k_2\left[Fe^{3+}\right][HP] - k_4[HP]\frac{k_1[Fe^{2+}] \quad [HP]}{k_4[HP] + k_5[\mathrm{PCT}] + k_6[HQ] + k_7[BQ]} \right] \right\} \tag{A.2}$$

$$\frac{dFe^{2+}}{dt} = -\frac{dFe^{3+}}{dt} = \frac{V_{irr}}{V_{tot}}\left\{ -k_1\left[Fe^{2+}\right][HP] + k_2\left[Fe^{3+}\right][HP] + \Phi_{Fe^{2+}}\left\langle \sum_\lambda e_\lambda^a\left(\underset{-}{x},t\right)\right\rangle_{V_{irr}} \right\} + \frac{V_{tot} - V_{irr}}{V_{tot}}\left\{ -k_1\left[Fe^{2+}\right][HP] + k_2\left[Fe^{3+}\right][HP] \right\} \tag{A.3}$$

$$\frac{dC_{HQ}}{dt} = \left\{ \frac{V_{irr}}{V_{tot}} \left[(k_5[\mathrm{PCT}] - k_6[\mathrm{HQ}])\frac{k_1[Fe^{2+}][HP] + \Phi_{Fe^{2+}}\left\langle \sum_\lambda e_\lambda^a\left(\underset{-}{x},t\right)\right\rangle_{V_{irr}}}{k_4[HP] + k_5[\mathrm{PCT}] + k_6[HQ] + k_7[BQ]} \right] \right\} + \left\{ \frac{V_{tot} - V_{irr}}{V_{tot}} \left[(k_5[\mathrm{PCT}] - k_6[\mathrm{HQ}])\frac{k_1[Fe^{2+}][HP]}{k_4[HP] + k_5[\mathrm{PCT}] + k_6[HQ] + k_7[BQ]} \right] \right\} \tag{A.4}$$

$$\frac{dC_{BQ}}{dt} = \left\{ \frac{V_{irr}}{V_{tot}} \left[(k_6[\mathrm{HQ}] - k_7[\mathrm{BQ}])\frac{k_1\left[Fe^{2+}\right][HP] + \Phi_{Fe^{2+}}\left\langle \sum_\lambda e_\lambda^a\left(\underset{-}{x},t\right)\right\rangle_{V_{irr}}}{k_4[HP] + k_5[\mathrm{PCT}] + k_6[HQ] + k_7[BQ]} \right] \right\} + \left\{ \frac{V_{tot} - V_{irr}}{V_{tot}} \left[(k_6[\mathrm{HQ}] - k_7[\mathrm{BQ}])\frac{k_1[Fe^{2+}][HP]}{k_4[HP] + k_5[\mathrm{PCT}] + k_6[HQ] + k_7[BQ]} \right] \right\} \tag{A.5}$$

Appendix B. Supporting information

Supplementary data associated with this article can be found in the online version at doi:10.1016/j.cattod.2022.11.019.

References

[1] P. Krzeminski, M.C. Tomei, P. Karaolia, A. Langenhoff, C.M.R. Almeida, E. Felis, F. Gritten, H.R. Andersen, T. Fernandes, C.M. Manaia, L. Rizzo, D. Fatta-Kassinos, Sci. Total Environ. 648 (2019) 1052–1081.
[2] A. Jurado, M. Walther, M.S. Díaz-Cruz, Sci. Total Environ. 663 (2019) 285–296.
[3] T.A. Ternes, C. Prasse, C.L. Eversloh, G. Knopp, P. Cornel, U. Schulte-Oehlmann, T. Schwartz, J. Alexander, W. Seitz, A. Coors, J. Oehlmann, Environ. Sci. Technol. 51 (2016) 308–319.
[4] G. Maniakova, K. Kowalska, S. Murgolo, G. Mascolo, G. Libralato, G. Lofrano, O. Sacco, M. Guida, L. Rizzo, Sep. Purif. Technol. 236 (2020), 116249.
[5] A. Das, M.K. Adak, Appl. Surf. Sci. Adv. 11 (2022), 100282.
[6] M. Antonopoulou, C. Kosma, T. Albanis, I. Konstantinou, Sci. Total Environ. 765 (2021), 144163.
[7] N. López-Vinent, A. Cruz-Alcalde, C. Lai, J. Giménez, S. Esplugas, C. Sans, Sci. Total Environ. 803 (2022), 149873.
[8] A. Shokry, F. Audino, P. Vicente, G. Escudero, M.P. Moya, M. Graells, A. Espuña, Modeling and Simulation of Complex Nonlinear Dynamic Processes Using Data Based Models: Application to Photo-Fenton Process, Elsevier, 2015.
[9] M. Pérez-Moya, M. Graells, P. Buenestado, H.D. Mansilla, Appl. Catal. B Environ. 84 (2008) 313–323.
[10] G.E. do Nascimento, M.A. Soares Oliveira, R.M. da Rocha Santana, B.G. Ribeiro, D. C. Silva Sales, J.M. Rodríguez-Díaz, D.C. Napoleão, M.A. da Motta Sobrinho, M.M. M.B. Duarte, Water Sci. Technol. 81 (2020) 2545–2558.
[11] A. Cabrera Reina, L. Santos-Juanes, J.L. García Sánchez, J.L. Casas López, M. I. Maldonado Rubio, G. Li Puma, J.A. Sánchez Pérez, Appl. Catal. B Environ. 166–167 (2015) 295–301.
[12] P. Soriano-Molina, J.L. García Sánchez, O.M. Alfano, L.O. Conte, S. Malato, J. A. Sánchez Pérez, Appl. Catal. B Environ. 233 (2018) 234–242.
[13] L.O. Conte, A.V. Schenone, B.N. Giménez, O.M. Alfano, J. Hazard. Mater. 372 (2019) 113–120.
[14] S. Park, S. Oh, Chemosphere 260 (2020), 127532.
[15] A. Spaltro, M.N. Pila, D.D. Colasurdo, E. Noseda Grau, G. Román, S. Simonetti, D. L. Ruiz, J. Contam. Hydrol. 236 (2021), 103739.
[16] A. Galani, N. Alygizakis, R. Aalizadeh, E. Kastritis, M.A. Dimopoulos, N. S. Thomaidis, Sci. Total Environ. 798 (2021), 149014.
[17] S. Wang, J. Wu, X. Lu, W. Xu, Q. Gong, J. Ding, B. Dan, P. Xie, Chem. Eng. J. 358 (2019) 1091–1100.
[18] G. Dalgic, F.I. TURKDOGAN, K. Yetilmezsoy, E. Kocak, Chem. Ind. Chem. Eng. Q 23 (2017) 177–186.
[19] P. Pal, R. Thakura, IEEE Int. Conf. Power, Control. Signals Instrum. Eng. ICPCSI 2017 (2018) 802–810.
[20] F. Audino, L.O. Conte, A.V. Schenone, M. Pérez-Moya, M. Graells, O.M. Alfano, Environ. Sci. Pollut. Res. 26 (2018) 4312–4323.
[21] R.F.P. Nogueira, M.C. Oliveira, W.C. Paterlini, Talanta 66 (2005) 86–91.
[22] E. Yamal-Turbay, E. Ortega, L.O. Conte, M. Graells, H.D. Mansilla, O.M. Alfano, M. Pérez-Moya, Environ. Sci. Pollut. Res. 22 (2014) 938–945.
[23] F. Audino, J.M.T. Santamaria, L.J. Del Valle Mendoza, M. Graells, M. Pérez-Moya, Int. J. Environ. Res. Public Health 16 (2019) 505.
[24] M. Pérez-Moya, T. Kaisto, M. Navarro, L.J. del Valle, Environ. Sci. Pollut. Res. 24 (2017) 6241–6251.
[25] M. Simunovic, H. Kusic, N. Koprivanac, A.L. Bozic, Chem. Eng. J. 173 (2011) 280–289.
[26] J.J. Pignatello, E. Oliveros, A. MacKay, Crit. Rev. Environ. Sci. Technol. 36 (2006) 1–84.
[27] B.N. Giménez, L.O. Conte, O.M. Alfano, A.V. Schenone, J. Photochem. Photobiol. A Chem. 397 (2020), 112584.
[28] L.O. Conte, J. Farias, E.D. Albizzati, O.M. Alfano, Ind. Eng. Chem. Res. 51 (2012) 4181–4191.
[29] I.B.A. Falconi, Marcela, P.G. Baltazar, D.C.R. Espinosa, Jorge, A.S. Tenório, B.A. Falconi, (2020).
[30] J.J. Plgnatello, Environ. Sci. Technol. 26 (1992) 944–951.
[31] M.I. Litter, Environ. Photochem. Part II 2 (2005) 325–366.
[32] E. De Laurentiis, C. Prasse, T.A. Ternes, M. Minella, V. Maurino, C. Minero, M. Sarakha, M. Brigante, D. Vione, Water Res 53 (2014) 235–248.
[33] H. Kusic, I. Peternel, S. Ukic, N. Koprivanac, T. Bolanca, S. Papic, A.L. Bozic, Chem. Eng. J. 172 (2011) 109–121.
[34] B.I. Escher, R. Baumgartner, J. Lienert, K. Fenner, Handb. Environ. Chem. Vol. 2 React. Process. 2 P (2009) 205–244.